IEICE TRANS. COMMUN., VOL.E106–B, NO.11 NOVEMBER 2023

INVITED PAPER *Joint Special Section on Opto-electronics and Communications for Future Optical Network*

40-GHz Band Photodiode-Integrated Phased Array Antenna Module for Analog-Radio over Fiber toward Beyond 5G

Shinji NIMURA †a), **Shota ISHIMURA** †, **Kazuki TANAKA**†, **Kosuke NISHIMURA** †, *and* **Ryo INOHARA**†, *Members*

SUMMARY In 5th generation (5G) and Beyond 5G mobile communication systems, it is expected that numerous antennas will be densely deployed to realize ultra-broadband communication and uniform coverage. However, as the number of antennas increases, total power consumption of all antennas will also increase, which leads to a negative impact on the environment and operating costs of telecommunication operators. Thus, it is necessary to simplify an antenna structure to suppress the power consumption of each antenna. On the other hand, as a way to realize ultra-broadband communication, millimeter waves will be utilized because they can transmit signals with a broader bandwidth than lower frequencies. However, since millimeter waves have a large propagation loss, a propagation distance is shorter than that of low frequencies. Therefore, in order to extend the propagation distance, it is necessary to increase an equivalent isotropic radiated power by beamforming with phased array antenna. In this paper, a phased antenna array module in combined with analog radio over fiber (A-RoF) technology for 40-GHz millimeter wave is developed and evaluated for the first time. An 8 × 8 phased array antenna for 40-GHz millimeter wave with integrated photodiodes and RF chains has been developed, and end-to-end transmission experiment including 20 km A-RoF transmission and 3-m over-the-air transmission from the developed phased array antenna has been conducted. The results showed that the 40-GHz RF signal after the end-to-end transmission satisfied the criteria of 3GPP signal quality requirements within ±50 degrees of main beam direction.

key words: *analog-radio over fiber (A-RoF), phased array antenna, beam forming, photo-mixing, 5G New Radio*

1. Introduction

Various use cases for Beyond 5G and 6G have been proposed and studied, such as autonomous driving [1], [2], holographic communication [3], extended reality (XR) [4], [5], and so on. Requirements for realizing these use cases are being discussed by many organizations [6]–[9]. Among them, ultra-broadband communication and uniform coverage are generally listed as key important properties of Beyond 5G and 6G. In order to realize uniform coverage, numerous antennas will be placed more densely to cover blind spots. However, it is necessary to consider that high-density placement of antennas will degrade signal quality due to radio wave interference between antennas. Centralized-radio access network (C-RAN) has been studied as one of the ways to solve this problem because it can suppress interference by operating geographically distributed antennas in coordination [10]–[12]. In order to coordinate antennas, it is necessary to connect numerous antennas to a single control unit via optical links called mobile fronthaul (MFH). Generally, digital-based MFH such as eCPRI is used as MFH for 5G [13]. In the current eCPRI-based antenna site configuration, several RAN functions are placed in the antenna site which includes low-layer PHY functions, digital-to-analog converter (DAC), analog-to-digital converter (ADC) and analog-based RF circuits. When massive numbers of antennas are distributed in the fields in Beyond 5G/6G era, total power consumption of these antennas will also increase, which will lead to a negative impact on the environment and operating costs to telecommunication operators. Thus, it is required to simplify the configuration and to reduce the power consumption of the antenna site equipment. A-RoF technology has been studied and considered as one of alternative solutions to the eCPRI-based MFH. In an A-RoF architecture, the radio signals are generated at a central office and transmitted to the antenna sites as an analog waveform, which contributes to reduce the digital signal processes at the antenna site and simplify the antenna site configurations. Typical A-RoF systems only utilize a simple intensity modulation and direct detection (IM-DD) scheme and have no digitizing function or the physical layer [14]–[17].

As a way to achieve ultra-broadband communication, on the other hands, millimeter waves (mmWaves) will be utilized in Beyond 5G and 6G because they can transmit signals with a broader bandwidth than lower frequencies such as sub-6 GHz (Sub6), which has been used in 5G and previous generations of mobile communication systems. It is well known that the propagation distance of mmWave is narrower than that of Sub6 due to its high attenuation by the atmosphere and obstructions. This limitation is compensated by using a phased array antenna, which increases an equivalent isotropic radiated power (EIRP) [18] to the specific direction by beamforming. Therefore, in order to meet both demands on a uniform coverage and an ultra-broadband communication at the same time, mmWave phased array antenna operating with A-RoF-based MFH architecture, i.e., photonic array antenna, will be required.

A number of photonic array antennas, in which photodiodes (PDs) and an array antenna are integrated, have been studied and reported so far. Typical previous studies focusing on mobile communications are summarized in Table 1. For example, Ref. [20]–[23] and [24]–[26] focus on the millimeter wave frequency bands defined by the 3rd genera-

Manuscript received January 6, 2023.
Manuscript revised April 7, 2023.
Manuscript publicized May 17, 2023.
†The authors are with KDDI Research, Inc., Fujimino-shi, 356-8502 Japan.
a) E-mail: sh-nimura@kddi.com
DOI: 10.1587/transcom.2022OBI0004

tion partnership project (3GPP) [19], 24.25–29.5 GHz and 57.0–71.0 GHz, respectively. Ref. [27] has been studied for even higher frequencies that are expected to be used in 6G. However, there are no reports of photonic array antennas that focus on 40-GHz band, which is specified in 3GPP and is expected to be fully deployed in 5G and later generations. Moreover, few reports have evaluated these photonic antennas using orthogonal frequency division multiplexing (OFDM) signal and quadrature amplitude modulation (QAM) for subcarrier modulation, which are the same modulation schemes as the radio signals for 3GPP-based mobile communication systems. Furthermore, from the respective of A-RoF transmission, there are few reports evaluating photonic array antennas over a 20-km fiber, which is the typical maximum transmission distance for MFH [28].

In this paper, we develop an 8×8 photonic array antenna for 40-GHz band with integrated PDs and RF chains, and conduct end-to-end downlink transmission experiments including 20-km A-RoF link and 3-m over-the-air link using 3GPP-compriant 64-QAM OFDM radio signals, for the first time. It has been confirmed that 40-GHz RF signal after end-to-end transmission satisfies the criteria of 3GPP signal quality requirements within ±50 degrees of main beam direction [29]. We also evaluate the power fading effect of the RF signal after A-RoF transmission, which is caused by chromatic dispersion of the single mode fiber (SMF). We introduce a scheme of generating RF signal by photo-mixing of A-RoF signal with a special spectrum relation to reduce the effect of the power fading, and apply it to perform end-to-end transmission experiment. This paper consists of 5 chapters. In Sect. 2, we introduce the design and structure of the developed photonic array antenna. In Sect. 3, we discuss the details of the experimental setup and the effect of power fading due to chromatic dispersion. In Sect. 4, we evaluate the signal quality under various conditions. Finally, Sect. 5 concludes the paper.

Table 1 Summary of previous studies.

Ref	Antenna elements	Output radio signal		A-RoF link (km)
		Center Frequency (GHz)	Modulation scheme	
[20]	16	28	64-QAM OFDM	1
[21]	4	28	64-QAM	0-25
[22]	4	28	64-QAM OFDM	2
[23]	64	28	16-QAM OFDM	N/A
[24]	8	60	16-QAM	0.05
[25]	20	60	16-QAM	2.2
[26]	32	60	16-QAM	10
[27]	32	300	QPSK OFDM	N/A

2. Design and Structure of Photonic Array Antenna

A block diagram and photograph of the developed photonic array antenna module are shown in Fig. 1 and Fig. 2, respectively. The antenna module had eight optical feeding lines and each line was connected to an independent RF chain. Each RF chain consisted of a high-speed PIN-PD, a low-noise amplifier (LNA), a variable attenuator, a variable phase shifter, a power amplifier (PA), a divider, and an 1×8 element patch array antenna. Specifications of each component are shown in Table 2. All variable attenuators and variable phase shifters are controlled individually from a computer via a control board. The A-RoF signal input to each optical feeding line was converted to an RF signal by a PIN-PD, and the amplitude and phase of the RF signal were adjusted by the variable attenuator and the variable phase shifter. After that, the RF signal was divided into eight by an eight-branch divider and fed to the patch array antenna with equal line lengths. The 1×8 element patch array antennas in the RF chain were spaced at half of a wavelength ($\lambda/2$) at 40 GHz. The measured radiation patterns of the 1×8 element patch array antennas for each RF chain when each RF chain was activated individually are shown in Fig. 3. For comparison, Fig. 3 also shows the result of numerical analysis of the radiation pattern in the elevation direction when the 1×8 element array antenna with the $\lambda/2$ element spacing is excited with the same phase. For reference, analysis results of the radiation pattern of a single patch antenna are shown in Fig. 4. From Fig. 3, both measured and calculated radiation patterns coincide well, and it could be said that our developed photonic array antenna

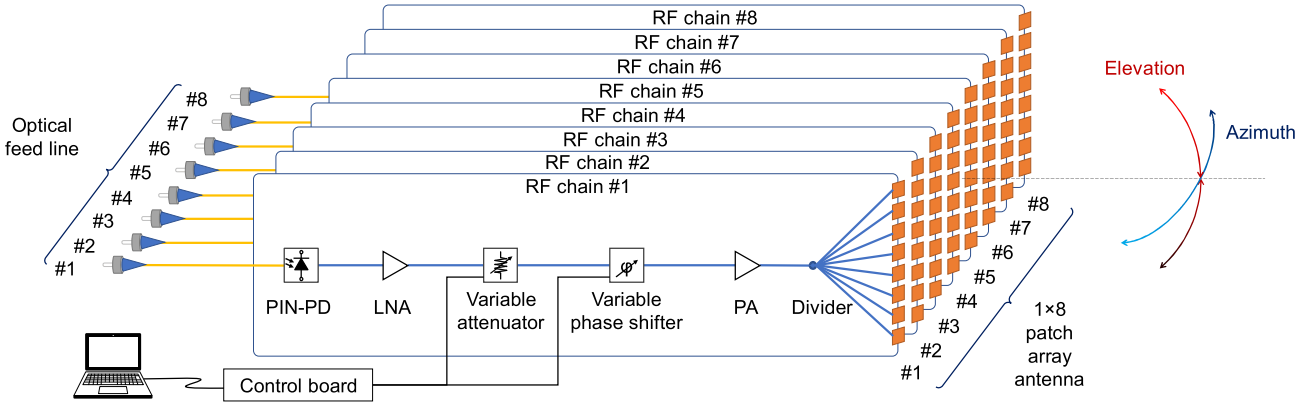

Fig. 1 Block diagram of internal structure of 8×8 photonic array antenna [29].

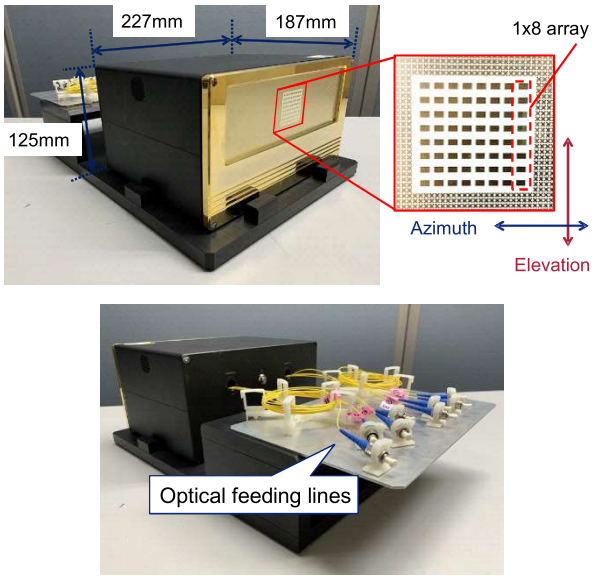

Fig. 2 Photographs of the exterior of 8 × 8 photonic array antenna.

Table 2 Specifications of each component.

Component	Parameter	Value
PIN-PD	3dB bandwidth	50 GHz
LNA	Gain	22 dB
	Noise figure	3.2 dB
PA	Gain	20 dB
Variable attenuator	Attenuation range	0-15.5 dB
	Attenuation steps	0.5 dB
Variable phase shifter	Shift range	0-355 degree
	Shift steps	5 degree

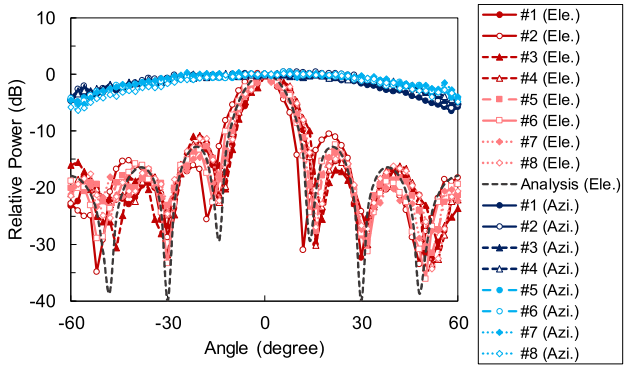

Fig. 3 Radiation pattern of each 1 × 8 element patch array antenna [29].

was well designed and fabricated to excite each antenna element with the same phase. The average measured gain of each 1 × 8 element patch array antenna was 11 dBi, and the elevation direction beam is fixed because of the limitation in the functionality of phase tuning in the sub-array of our developed antenna. An 8 × 8 element patch array antenna was constructed by lining 1 × 8 element patch array antennas side-by-side with λ/2 spacing in the horizontal direction. The azimuth direction beam can be controlled by adjusting the phase difference between the RF chains using variable phase shifters. The measured and analyzed radiation patterns of the 8 × 8 antenna at 0 degrees are shown in Fig. 5, and the analyzed radiation patterns from −50 to 50 degrees are shown in Fig. 6. From Fig. 5, it can be confirmed that the measured and analyzed radiation patterns coincide well. For this reason, it is expected that radiation patterns as shown in Fig. 6 can be obtained at other angles as well. The measured gain of the 8 × 8 element patch array antenna at 0 degrees was 20 dBi.

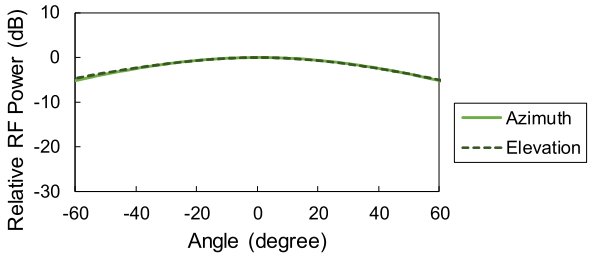

Fig. 4 Analyzed radiation pattern of a single element antenna.

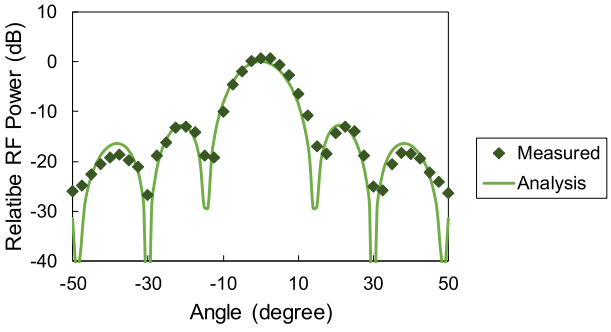

Fig. 5 Measured and Analyzed radiation patterns in the azimuth direction of 8 × 8 element patch array antenna.

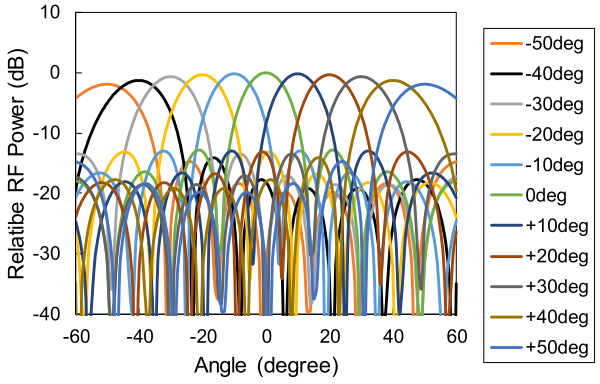

Fig. 6 Analyzed radiation pattern in the azimuth direction of 8 × 8 element patch array antenna.

3. Experimental Setup

3.1 Configuration

The experimental setup to evaluate the performance of the developed photonic array antenna was shown in Fig. 7. A-RoF signal was generated using a distributed feedback laser

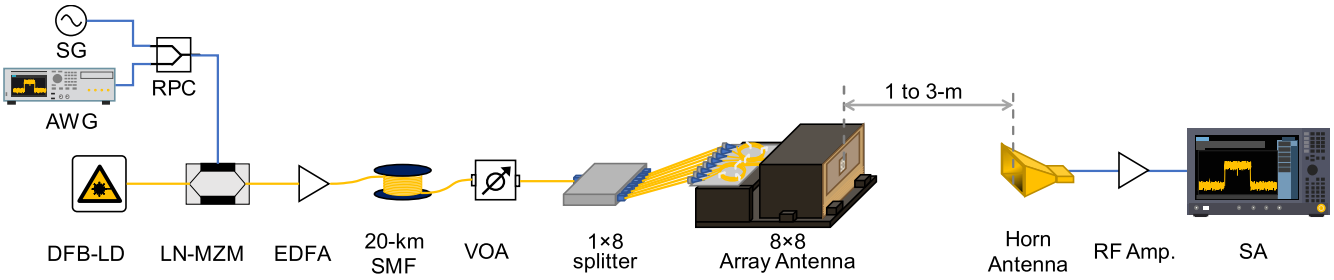

Fig. 7 Experimental setup to evaluate signal qualities [29].

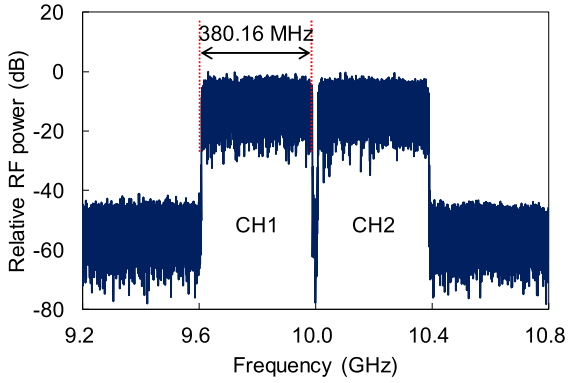

Fig. 8 RF spectrum output from AWG.

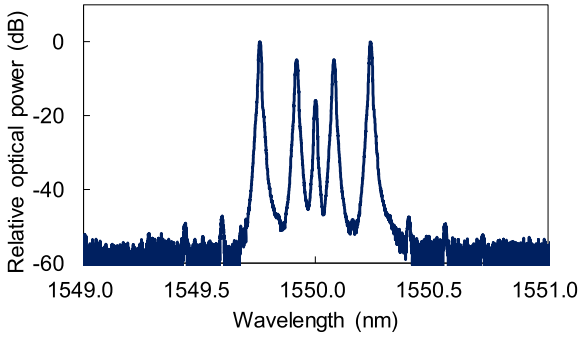

Fig. 9 Optical spectrum output from LN-MZM.

diode (DFB-LD) and a lithium niobate Mach-Zender modulator (LN-MZM) with a half-wave voltage of 1.7 V and a chirp parameter of approximately 0. In order to alleviate the bandwidth requirement of the LN-MZM, a signal generator (SG), and an arbitrary waveform generator (AWG) for 40-GHz A-RoF signal generation, two types of low-frequency RF signal components with their sum of frequency equals to 40 GHz were input to the LN-MZM so that the 40-GHz RF signal could be obtained by photo-mixing of the photodetector in the photonic array antenna at the receiver side. Thus, a continuous wave signal of 30 GHz generated by the SG and a radio signal of 10 GHz generated by the AWG were combined by a resistive power combiner (RPC) as the modulation signal for A-RoF. The detailed frequency relation of the modulated and the continuous wave signal were described in Sect. 3.2. To minimize error vector magnitude (EVM), the average power of the continuous wave signal and the radio signal were set to 12.4 dBm and 0.9 dBm, respectively. As shown in Fig. 8, the radio signal used a two-channel 64-QAM OFDM signal to simulate intra-band contiguous carrier aggregation. The signal bandwidth, subcarrier spacing, and number of subcarriers for each signal were 380.16 MHz, 120 kHz, and 3168, respectively. The center frequency of each channel was set to ±0.2 GHz relative to the center frequency of the radio signal. The low-frequency and high-frequency 64-QAM OFDM signals were defined as CH1 and CH2, respectively. EVMs of CH1 and CH2 at the output from the AWG were 1.0% and 1.1%, respectively. As shown in Fig. 9, the optical carrier component, which was not used for the demodulation in this experiment, was suppressed by adjusting the bias voltage to avoid saturation of the erbium-doped fiber amplifier (EDFA). The A-RoF signal output from the LN-MZM was amplified by EDFA and transmitted over a 20-km SMF. An optical variable attenuator (VOA) was used to adjust the input optical power to photonic array antenna, and the A-RoF signal was distributed to each RF chain with a 1×8 optical splitter. We could split the received A-RoF signal in electrical domain, however, to reduce the power consumption in the remote antenna site as much as possible, we used the passive optical splitter to feed the received signal to each RF chain. Each PIN-PD outputs the beat components of the input A-RoF signal. However, only the signals in the 40-GHz band, i.e. the beat component of radio and continuous wave signal, were output from the developed photonic array antenna because amplifiers in the RF chains had a frequency characteristic that only amplified signals around 40 GHz. The center frequencies of CH1 and CH2 after the photo detection were 39.8 GHz and 40.2 GHz, respectively. Phases of the radio signals were controlled by variable phase shifters and adjusted to obtain maximum power for a specific direction. The values of the variable attenuators were adjusted to the minimum in order to reduce the effect of attenuation by the RF chains. The radio signal radiating from the 8×8 elements patch array antenna was received by a horn antenna placed at a distance 1 to 3-m from the developed antenna. Since the expected minimum distance from the base station to the user terminal is 2-m for the local area base station [19], the distance between antennas was set to be 1 to 3-m around that distance. The received RF signal was amplified by an RF amplifier, and EVM was evaluated using a signal

analyzer (SA).

3.2 Optimization of Photo-Mixing Frequencies

In this section, the power fading effect, which occurs for intensity-modulated A-RoF signal under the presence of chromatic dispersion and could degrade the received signal quality especially for longer transmission distance, is explained and experimentally evaluated. In order to generate a 40-GHz signal by photo-mixing, two signals that the sum of the center frequencies is 40 GHz are input to the intensity modulator. When the optical carrier frequency is f_0 and the center frequencies of the two signals are f_1 and f_2, respectively, an optical spectrum of an A-RoF obtained by the modulator is shown in Fig. 10(a). When this A-RoF signal is input to the PIN-PD, the PIN-PD outputs an electrical signal that generates the beats of the lower sideband (LSB) of f_1 and the upper sideband (USB) of f_2 (beat 1) and the beats of the LSB of f_2 and the USB of f_1 (beat 2). However, when the A-RoF signal is transmitted over a typical SMF, a phase difference φ between beats 1 and 2 was imposed because the propagating speed of each spectrum component differs due to chromatic dispersion, as shown in Fig. 10(b). This phase difference causes power fading and its effect varies depending on the combination of f_1 and f_2 and on fiber parameters

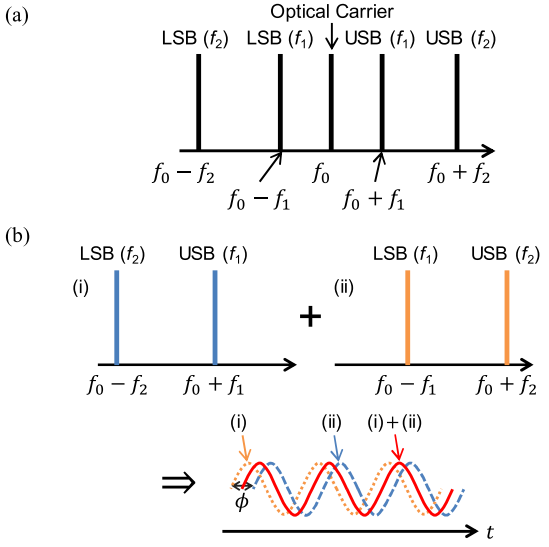

Fig. 10 Image of signal generation by photo-mixing.

such as a chromatic dispersion coefficient and fiber length. The effect of power fading due to chromatic dispersion for a typical A-RoF signal is

$$P \propto \left|\cos\left(\frac{\pi\lambda_{opt}^2 dLf^2}{c}\right)\right|^2, \tag{1}$$

where P is a power output from the PIN-PD, λ_{opt} is an optical wavelength, d is the chromatic dispersion coefficient, L is the fiber length, f is a radio signal frequency, and c is a light velocity. However, Eq. (1) cannot be applied directly to this experiment because we use photo-mixing and two components with different frequencies are input to the modulator. Therefore, we experimentally determined the combination of frequencies that minimizes the effect of chromatic dispersion. The experimental system is shown in Fig. 11. The configuration from DFB-LD to VOA was the same as the experimental system in Fig. 7. In order to ease confirmation of the effects of power fading, another SG was used instead of the AWG. Each SG is defined as SG1 and SG2, respectively. In addition, a PIN-PD was used instead of the developed photonic array antenna in this evaluation. The center frequency of SG1 was set to be between 9 and 19 GHz and the center frequency of SG2 was set to be between 21 and 31 GHz, so that the sum of both frequencies was always 40 GHz. The generated A-RoF signal was transmitted over the 20-km SMF, and the level was adjusted by the VOA so that the received optical power of the PIN-PD was always constant. The output power of the PIN-PD was evaluated by extracting only the 40-GHz output using a band pass filter (BPF) and inputting it into a power meter. The measured output power versus center frequency for SG1 and SG2 was shown in Fig. 12. The power fading effect was observed as the output power attenuation when the combination of the center frequency of SG1 and SG2 was changed. It was confirmed that the maximum output power was obtained when the center frequency of SG1 was around 10 GHz and 15 GHz. Considering these results and the bandwidths of the LN-MZM, the SG, and the AWG used in this paper, the center frequencies of the SG and the AWG in the experimental system in Fig. 7 were set to 30 GHz and 10 GHz, respectively.

4. Experimental Results and Discussion

We evaluated the developed photonic array antenna includ-

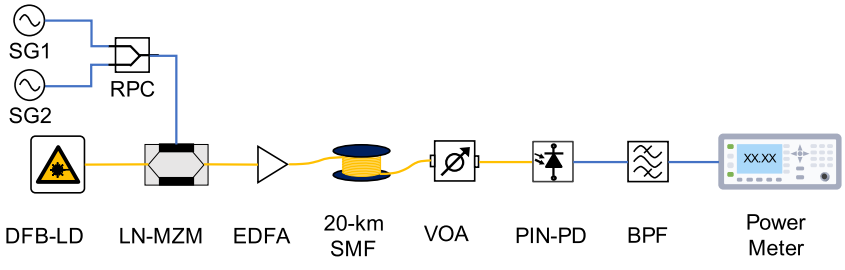

Fig. 11 Experimental setup to evaluate the effect of chromatic dispersion.

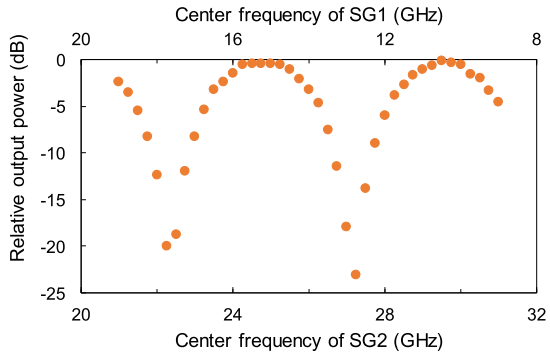

Fig. 12 Measured output power for each center frequency.

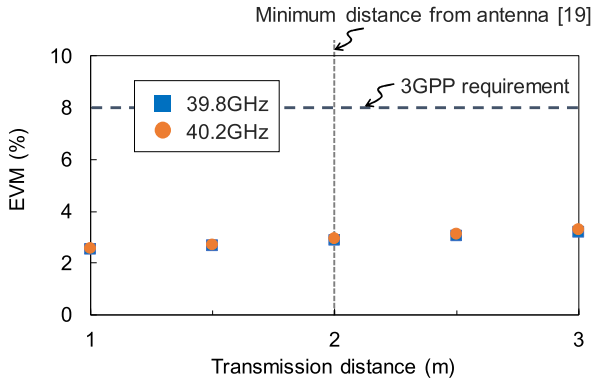

Fig. 13 EVM for various free-space transmission distance [29].

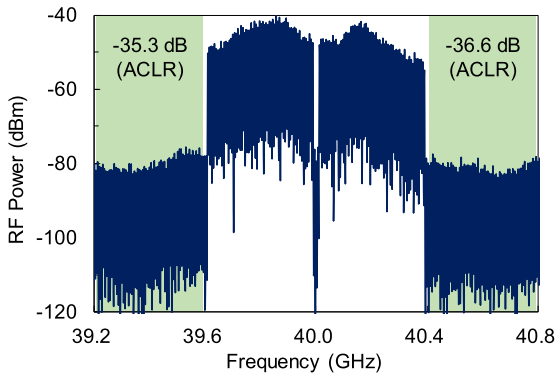

Fig. 14 RF spectrum after 20-km A-RoF transmission and 3-m free-space propagation [29].

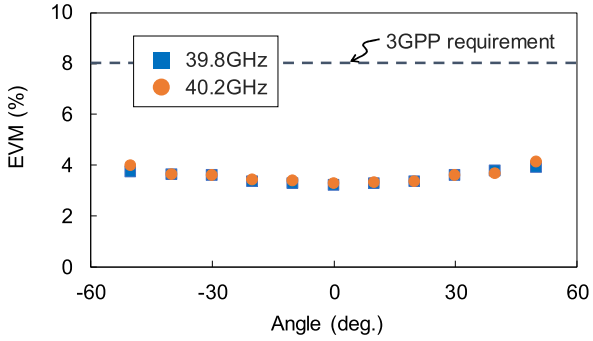

Fig. 15 EVMs for various main beam direction [29].

ing 20-km A-RoF transmission and over-the-air transmission for different free-space transmission distance, the main beam direction, and the received optical power of the A-RoF signal.

The EVMs for various propagation distance in free-space and the measured RF spectrum at a free-space transmission distance of 3-m were shown in Fig. 13 and Fig. 14, respectively. Note that Fig. 14 was measured with resolution bandwidth and video bandwidth of the spectrum analyzer set to 10 kHz. The main beam direction was set to 0 degrees, and the received optical power of each PIN-PD was set to −5.4 dBm/PD to obtain minimum EVMs. The output power from the antenna under these conditions was 17 dBm including EIRP, which satisfied the requirement of less than 33 dBm, the upper power limit for local area base stations defined by 3GPP [19]. The received power excluding the gain of the horn antenna and the RF amplifier was −48 to −57 dBm. As shown in Fig. 13, the EVMs were gradually degraded with increasing free-space propagation distance, and the values of 3.2% for CH1 and 3.3% for CH2 were obtained at 3-m. However, there were sufficient margins for EVM 8%, which is the signal quality requirement for 64-QAM OFDM signal [19]. Furthermore, Fig. 14 showed that the adjacent channel leakage power ratio (ACLR) was less than −35.3 dB, which fully satisfies the ACRL limit of less than −26 dB required in the 40-GHz band [19]. Although the free-space propagation distance couldn't be extended beyond 3-m due to the limitations of the experimental environment, it was confirmed that the developed photonic array antenna has sufficient performance to propagate over longer distance while meeting 3GPP requirements.

The EVMs for various main beam directions in the range of −50 to 50 degrees, which was the maximum controllable angle of the developed photonic array antenna, are shown in Fig. 15. The free-space propagation distance was set to 3-m, and the received optical power of each PIN-PD was set to −5.4 dBm/PD. The angle between the array antenna and the horn antenna in the elevation direction was set to 0 degree, and the developed photonic array antenna was rotated in the azimuth direction. Each variable phase shifter was adjusted so that the main beam direction was toward the horn antenna. As shown in Fig. 15, the EVMs were minimum at 0 degrees and degraded slightly with increasing angle. However, there was a sufficient margin for 8%. In addition, we compared the EVMs of angles with equal absolute values and confirmed that the difference was within 0.2 percentage points. Thus, these results showed that good symmetry properties could be obtained.

Finally, to confirm the dynamic range of the received A-RoF signal power, the EVM was evaluated when the received optical power of the PIN-PD was changed. The free-space propagation distance was set to 3-m, and the main beam direction was set to 0 degrees. In this case, the output power changed by 2 dB when the received optical power was changed by 1 dB. The results are shown in Fig. 16. The

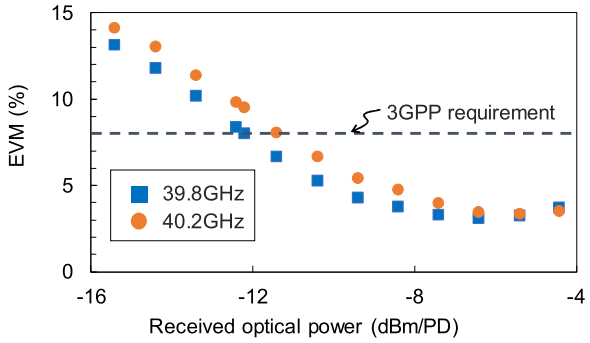

Fig. 16 EVMs for various received optical power [29].

EVM of CH2 reached 8% when the received optical power was −11.4 dBm/PD. On the other hand, the EVM on the higher power side has enough margin for 8%. Although the received optical power could not be increased above −4 dBm/PD due to the limitation of the EDFA output, it was confirmed that a dynamic range of more than 7 dB could be obtained. From these results and the fact that the transmission loss of the SMF in C-band is typically less than 0.35 dB/km, it was shown that it has a sufficient dynamic range to accommodate various fiber lengths from a few kilometers up to 20-km.

5. Conclusion

In this paper, the 8 × 8 photonic array antenna module for 40-GHz band with beamforming function for A-RoF-based MFH architecture was developed and demonstrated, for the first time. The EVMs were evaluated after 20-km A-RoF transmission and 3-m free-space propagation using the 3GPP-compliant two-channel 64-QAM OFDM signal. As a result, it was confirmed that all EVMs satisfied the 3GPP signal quality requirement within ±50 degrees in the main beam direction, and good symmetry beam characteristics were obtained. These results showed that our proposed photodiode-integrated phased array antenna could transmit the radio signal at 40 GHz in conjunction with A-RoF-based mobile fronthaul link up to 20 km with meeting the 3GPP signal quality criteria.

Acknowledgments

This work was partly supported by “Research and Development of Optical Access Infrastructure for Accommodating Large Capacity Traffic Toward Beyond 5G Mobile Systems”, the Commissioned Research of National Institute of Information and Communications Technology (NICT), JAPAN. We thank TMY Technology, Inc. for their assistance in the development and evaluation.

References

[1] J. Kim, Y.-J. Choi, G. Noh, and H. Chung, “On the feasibility of remote driving applications over mmWave 5G vehicular communications: Implementation and demonstration,” IEEE Trans. Veh. Technol., vol.72, no.2, pp.2009–2023, 2023, DOI: 10.1109/TVT.2022.3210689.

[2] T. Taleb, N. Sehad, Z. Nadir, and J. Song, “VR-based immersive service management in B5G mobile systems: A UAV command and control use case,” IEEE Internet Things J., vol.10, no.6, pp.5349–5363, 2023, DOI: 10.1109/JIOT.2022.3222282.

[3] E.C. Strinati, S. Barbarossa, J.L. G.-Jimenez, D. Kténas, N. Cassiau, L. Maret, and C. Dehos, “6G: The next frontier: From holographic messaging to artificial intelligence using subterahertz and visible light communication,” IEEE Veh. Technol. Mag., vol.14, no.3, pp.42–50, Sept. 2019, DOI: 10.1109/MVT.2019.2921162.

[4] S. Rostami and M. Maier, “The metaverse and beyond: Implementing advanced multiverse realms with smart wearables,” IEEE Access, vol.10, pp.110796–110806, 2022, DOI: 10.1109/ACCESS.2022.3215736.

[5] S. Rostami and M. Maier, “The metaverse and beyond: Implementing advanced multiverse realms with smart wearables,” IEEE Access, vol.10, pp.110796–110806, 2022, DOI: 10.1109/ACCESS.2022.3215736.

[6] “Beyond 5G White Paper~Message to the 2030s~version 1.51,” Beyond 5G Promotion Consortium, https://b5g.jp/doc/whitepaper_en_1-51.pdf, accessed Nov. 2022.

[7] “Next G alliance report: Roadmap to 6G,” Next G Alliance, https://www.nextgalliance.org/wp-content/uploads/2022/02/NextGA-Roadmap.pdf, accessed Nov. 2022.

[8] “Key drivers and research challenges for 6G ubiquitous wireless intelligence,” 6G FLAGSHIP, http://jultika.oulu.fi/files/isbn9789526223544.pdf, accessed Nov. 2022.

[9] “White paper on 6G vision and candidate technologies,” IMT-2030 (6G) Promotion Group, http://www.caict.ac.cn/english/news/202106/P020210608349616163475.pdf, accessed Nov. 24. 2022.

[10] A.M. Alba, S. Janardhanan, and W. Kellerer, “Enabling dynamically centralized RAN architectures in 5G and beyond,” IEEE Trans. Netw. Service Manag., vol.18, no.3, pp.3509–3526, Sept. 2021, DOI: 10.1109/TNSM.2021.3071975.

[11] H.Q. Ngo, A. Ashikhmin, H. Yang, E.G. Larsson, and T.L. Marzetta, “Cell-free massive MIMO versus small cells,” IEEE Trans. Wirel. Commun., vol.16, no.3, pp.1834–1850, March 2017, DOI: 10.1109/TWC.2017.2655515.

[12] M. Ito, I. Kanno, K. Yamazaki, Y. Kishi, W.-Y. Chen, T. Choi, and A.F. Molisch, “Impact of antenna distribution on spectral and energy efficiency of cell-free massive MIMO with transmit power control algorithms,” IEEE Open J. Commun. Soc., vol.3, pp.1615–1629, 2022, DOI: 10.1109/OJCOMS.2022.3209952.

[13] Common Public Radio Interface, eCPRI Specification V2.0, May 2019.

[14] K. Nishimura, S. Ishimura, H.-Y. Kao, K. Tanaka, and R. Inohara, “Scalability of A-RoF based mobile fronthaul toward beyond-5G,” Proc. 2021 Opto-Electron. and Commun. Conf. (OECC), pp.1–3, Oct. 2021.

[15] K. Tanaka, H.-Y. Kao, S. Ishimura, K. Nishimura, T. Kawanishi, and M. Suzuki, “Cascaded IF-over-fiber links with hybrid signal processing for analog mobile fronthaul,” J. Light. Technol., vol.38, no.20, pp.5656–5667, Oct. 2020, DOI: 10.1109/JLT.2020.3001930.

[16] K. Kanta, A. Pagano, E. Ruggeri, M. Agus, I. Stratakos, R. Mercinelli, C. Vagionas, P. Toumasis, G. Kalfas, G. Giannoulis A. Miliou, G. Lentaris, D. Apostolopoulos, N. Pleros, D. Soudris, and H. Avramopoulos, “Analog fiber-wireless downlink transmission of IFoF/mmWave over in-field deployed legacy PON infrastructure for 5G fronthauling,” J. Opt. Commun. Netw., vol.12, no.10, pp.D57–D65, Oct. 2020, DOI: 10.1364/JOCN.391803.

[17] H. Yasuda, T. Aiba, S. Tanaka, T. Suzuki, S. Ishimura, K. Tanaka, K. Nishimura, H.-Y. Kao, T. Wakabayashi, and T. Kawanishi, “800-MHz bandwidth signal transmission with radio over multi-mode-fiber for cascaded IFoF-based C-RAN mobile fronthaul,” J. Lightw. Technol., vol.39, no.24, pp.7716–7725, Dec. 2021, DOI: 10.1109/JLT.2021.3103500.

[18] T. Nagayama, S. Akiba, T. Tomura, and J. Hirokawa, "Photonics-based millimeter-wave band remote beamforming of array-antenna integrated with photodiode using variable optical delay line and attenuator," J. Lightw. Technol., vol.36, no.19, pp.4416–4422, Oct. 2018, DOI: 10.1109/JLT.2018.2821185.
[19] "Base station (BS) radio transmission and reception," 3GPP TS 38.104, ver. 17.7.0, Aug. 2022.
[20] H.-Y. Kao, S. Ishimura, K. Tanaka, K. Nishimura, and R. Inohara, "Photodiode-integrated array-antenna module enabling 2-D beamforming for RoF transmission," 2020 Opto-Electron. and Commun. Conference (OECC), Oct. 2020, pp.1–3, DOI: 10.1109/OECC48412.2020.9273442.
[21] M.-Y. Huang, Y.-W. Chen, P.-C. Peng, H. Wang, and G.-K. Chang, "A full field-of-view self-steering beamformer for 5G mm-Wave fiber-wireless mobile fronthaul," J. Lightw. Technol., vol.38, no.6, pp.1221–1229, March 2020, DOI: 10.1109/JLT.2019.2956667.
[22] L. Bogaert, J.V. Kerrebrouck, H. Li, I.L. de Paula, K. Van Gasse, C.-Y. Wu, P. Ossieur, S. Lemey, H. Rogier, P. Demeester, G. Roelkens, J. Bauwelinck, and G. Torfs., "SiPhotonics/GaAs 28-GHz transceiver with reflective EAM for laser-less mmWave-over-fiber," J. Lightw. Technol., vol.39, no.3, pp.779–786, Feb. 2021, DOI: 10.1109/JLT.2020.3021175.
[23] X. Li, P. (B.) Shih, Q. Ji, H. (K.) Huang, S.T. Abraha, C. Kim, D.R. Peters, D.F. Castellana, and A. Ng'oma, "28-GHz mmWave hybrid beamforming system integrated with a 64-element glass antenna," 2021 Optical Fiber Commun. Conf. and Exhibition (OFC), pp.1–3, June 2021. DOI: 10.1364/OFC.2021.M3J.3
[24] T. Nagayama, S. Akiba, T. Tomura, and J. Hirokawa, "Photonics-based millimeter-wave band remote beamforming of array-antenna integrated with photodiode using variable optical delay line and attenuator," J. Lightw. Technol., vol.36, no.19, pp.4416–4422, Oct. 2018, DOI: 10.1109/JLT.2018.2821185.
[25] U. Habib, M. Steeg, A. Stöhr, and N.J. Gomes, "Single radio-over-fiber link and RF chain-based 60 GHz multi-beam transmission," J. Lightw. Technol., vol.37, no.9, pp.1974–1980, May 2019, DOI: 10.1109/JLT.2019.2896778.
[26] E. Ruggeri, A. Tsakyridis, C. Vagionas, G. Kalfas, R.M. Oldenbeuving, P.W. L. van Dijk, C.G.H. Roeloffzen, Y. Leiba, N. Pleros, and A. Miliou, "A 5G fiber wireless 4 Gb/s WDM fronthaul for flexible 360° coverage in V-band massive MIMO small cells," J. Lightw. Technol., vol.39, no.4, pp.1081–1088, Feb. 2021, DOI: 10.1109/JLT.2020.3029608.
[27] J. Tebart, P. Lu; T. Haddad, S. Iwamatsu, J. Lackmann, J.L. F.-Estevez, and A. Stöhr, "Mobile terahertz 6G communications enabled by integrated photonic-assisted beam steering antennas," 2021 European Conf. on Optical Commun. (ECOC), pp.1–3, Sept. 2021, DOI: 10.1109/ECOC52684.2021.9605939.
[28] ITU-T G Suppl. 66, "5G wireless fronthaul requirement in a passive optical network context, 2019.
[29] S. Nimura, S. Ishimura, K. Tanaka, K. Nishimura, and R. Inohara, "Photodiode-integrated 8×8 array-antenna module for analog-RoF supporting 40-GHz 5G systems," 2022 27th OptoElectron. and Commun. Conf. (OECC) and 2022 International Conf. on Photonics in Switching and Computing (PSC), pp.1–4, July 2022, DOI: 10.23919/OECC/PSC53152.2022.9849912.
[30] F. Devaux, Y. Sorel, and J.F. Kerdiles, "Simple measurement of fiber dispersion and of chirp parameter of intensity modulated light emitter," J. Lightw. Technol., vol.11, no.12, pp.1937–1940, Dec. 1993, DOI: 10.1109/50.257953.

Shinji Nimura received the B.S. and M.S. degrees in electrical and electronic information engineering from the Toyohashi University of Technology, Aichi, Japan, in 2018 and 2020, respectively. He joined KDDI Research, Inc., Saitama, Japan, in 2021, and has been engaged in research on optical access networks. He received Best Paper Award at the 27th Opto-Electronics and Communications Conference (OECC) in 2022. He is a member of the Institute of Electronics, Information and Communication Engineers (IEICE).

Shota Ishimura received his B.E. degree in Electrical Engineering from Tokyo University of Agriculture and Technology in 2013 and M.E. and Ph.D. degrees in Engineering from the University of Tokyo in 2015 and 2021, respectively. He joined KDDI R&D Laboratories, Inc. (currently KDDI Research, Inc.), Saitama, Japan, in 2016, and has been engaged in research on optical access networks. He is a member of the Institute of Electronics, Information and Communication Engineers (IEICE).

Kazuki Tanaka received the B.E. and M.E. degrees in applied physics and the Dr.Eng. degree in electronic and physical systems from Waseda University, Tokyo, Japan, in 2004, 2006, and 2021, respectively. He joined KDDI Research, Inc., Saitama, Japan, in 2006, and has been engaged in research on optical access networks and microwave photonics. He is a member of the Institute of Electronics, Information and Communication Engineers (IEICE).

Kosuke Nishimura received B.E., M.S. and Ph.D. degrees in electrical engineering from Tokyo Institute of Technology, Tokyo, Japan in 1986, 1988, and 2008, respectively. Since 1988, he has been with KDDI Research, Inc., Saitama, Japan, where he has studied visible light emitting materials, all-optical functional devices, and new applications utilizing electronic paper display. Currently, he is engaged in the research and development of technologies for optical and wireless convergence toward Beyond 5G. He is a member of Society for Information Display (SID), Japan Society of Applied Physics (JSAP), and Institute of Electronics, Information and Communication Engineers (IEICE).

Ryo Inohara received B.E. and M.E. degrees in Communications Engineering from Osaka University, Osaka, Japan, in 1999 and 2001, respectively. He joined KDDI R&D Laboratories, Inc. in 2001, where he has studied all-optical signal processing and home network technology. Currently, he is a senior manager of optical access network laboratory at KDDI Research, Inc. and engaged in the research and development of optical access network technologies toward Beyond 5G. He is a member of the Institute of Electronics, Information and Communication Engineers (IEICE).